

AD663584

Loan Copy.  
Pls return to  
C008467, ONR

Fourth Semi-Annual Status Report  
STUDY OF UNDERWATER  
SOUND PROJECTORS

Contract No. NONR 4741(00) ✓



**FAIRCHILD HILLER**  
REPUBLIC AVIATION DIVISION  
FARMINGDALE, LONG ISLAND, NEW YORK

Reproduced by the  
**CLEARINGHOUSE**  
for Federal Scientific & Technical  
Information Springfield, Va. 22151

PC088R0001  
FHR 2229-4  
PCD-TR-67-7  
30 June 1967

Fourth Semi-Annual Status Report

STUDY OF UNDERWATER  
SOUND PROJECTORS

Contract No. NONR 4741(00) ✓

FHR 2229-4

by

William J. Guman  
Burton Humphrey

Prepared for:  
Acoustics Program  
Naval Applications Group  
Office of Naval Research  
Washington, D. C. 20360

FAIRCHILD HILLER CORPORATION  
REPUBLIC AVIATION DIVISION  
Farmingdale, New York 11735

## CONTENTS

<u>Section</u>		<u>Page</u>
I	BRIEF INTRODUCTION	1
II	LOW INDUCTANCE DISCHARGE CIRCUIT	2
	A. Construction Details	2
	B. Experimental Results	10
III	FREQUENCY SPECTRUM SHAPING	17
	A. Introduction	17
	B. Experimental Arrangement	18
Appendix A.	Spectral Analysis of Pressure Traces Resolvable as Connected Straight Line Segments	25

## SECTION I - BRIEF INTRODUCTION

In the last progress report<sup>1</sup> it was concluded that a low inductance electric network should convert more of the available electric energy into acoustic energy than the high inductance networks that have been used previously. It is essential, however, that in either type of network the interelectrode spacing of the electrodes be adjusted to produce a critically-damped discharge.

The low inductance discharge circuit described in the last report<sup>1</sup> was assembled and tested in water of zero salinity. This progress report describes results obtained with the low-inductance discharge circuit and presents some recommendations to be followed in assembling future low-inductance electric discharge acoustic sources.

A versatile pulse-forming network to be used in the near future with the inverse-pinch acoustic sound source has been designed and bench checked. This latter discharge network and some of its features are also described in this report.

## SECTION II - LOW INDUCTANCE DISCHARGE CIRCUIT

The assembled low inductance discharge circuit acoustic sound source is shown in Figure 1. A schematic of the associated electric circuitry that was used to charge the capacitor bank and to discharge the capacitively stored energy into the electrode assembly is presented in Figure 2.

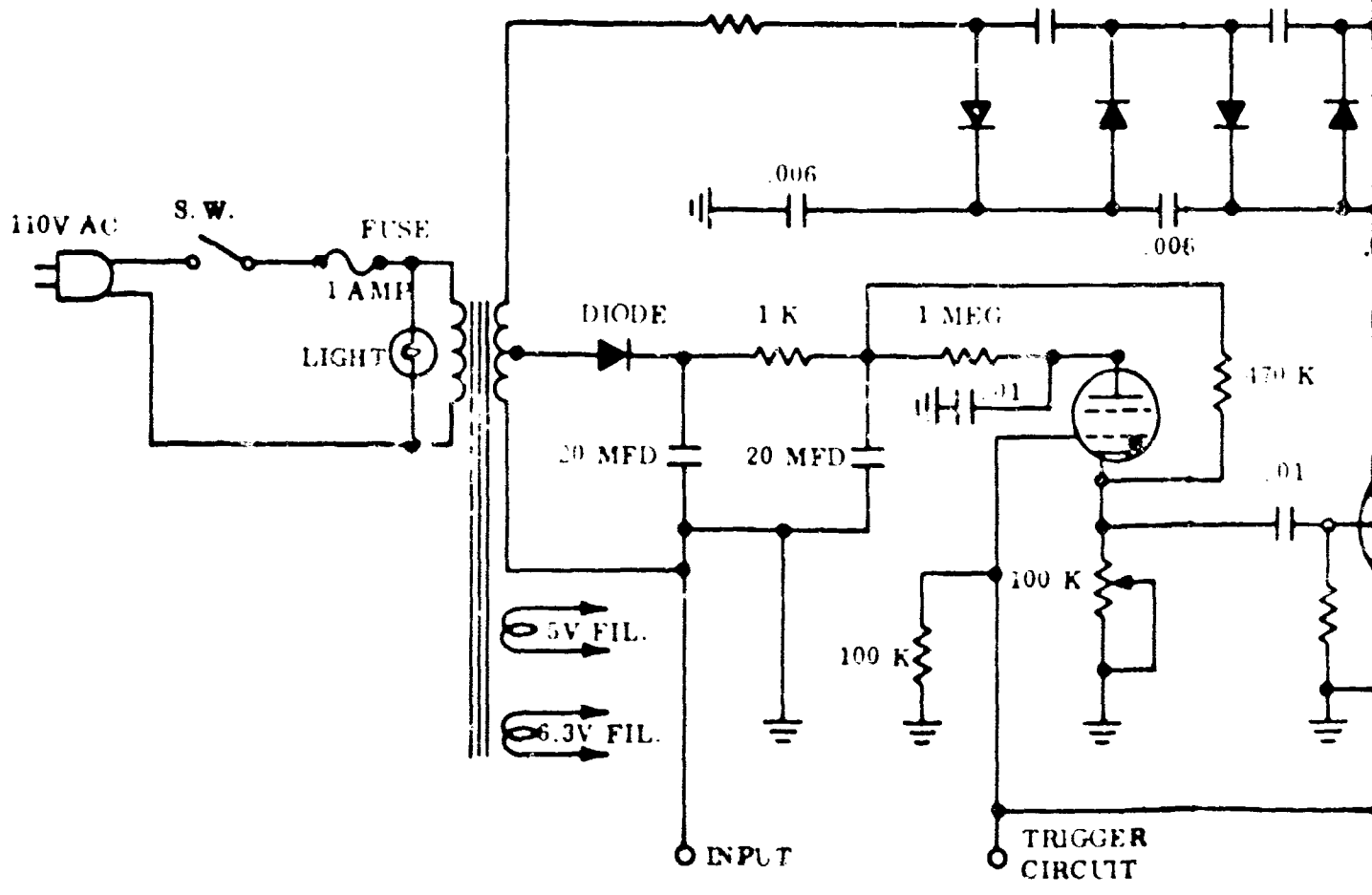
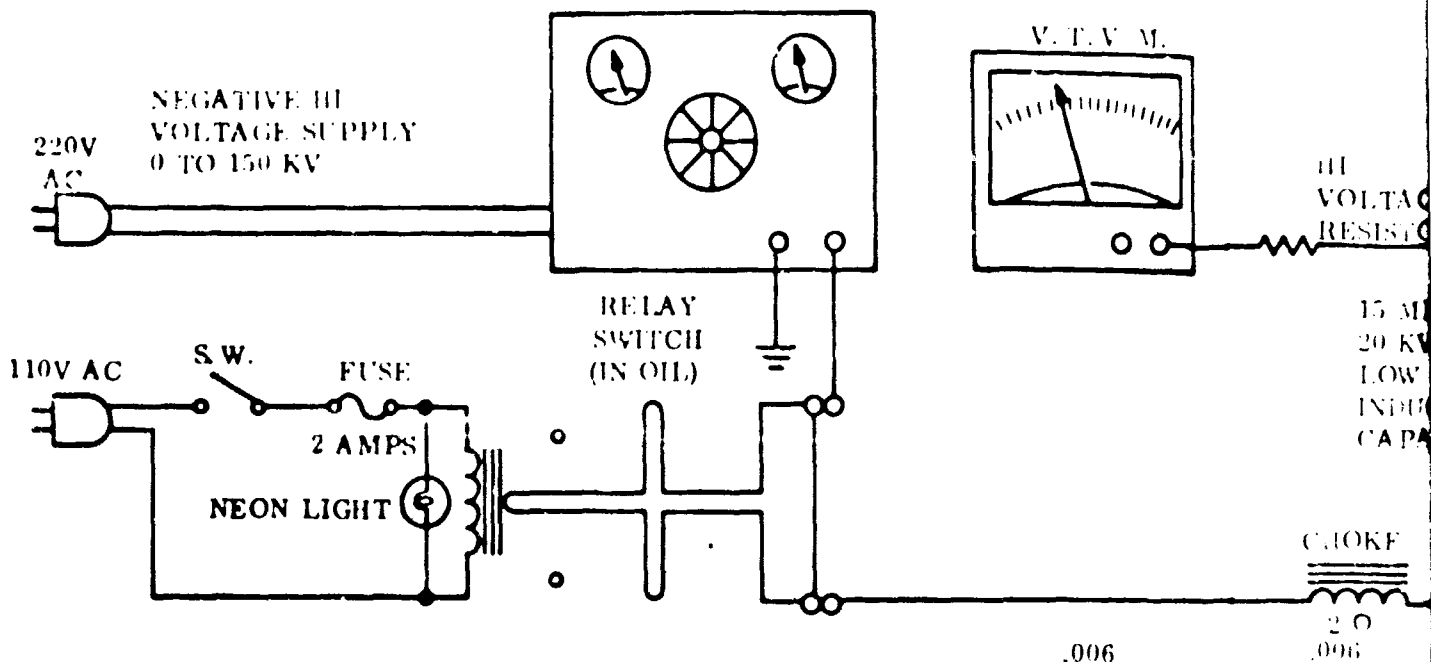
### A. CONSTRUCTION DETAILS

Originally the inverse-pinch electrode assembly of the low inductance network was fastened directly to the ignitron, the ignitron being attached directly to the outlet bushings of the capacitor. This arrangement is shown in Figure 3. This latter arrangement was mechanically quite rigid. During operation the entire capacitor and electrode assembly was submerged in water and it was found that the pressure field generated by the electric discharge at the 3000 joule energy level caused a sufficiently large axial pressure force to be exerted against the electrode assembly to break the glass envelope within the G.E. GL 7703 ignitron. The assembly was therefore redesigned incorporating a flexible bellows in the line between the ignitron and the electrode assembly. While this technique did not lead to another ignitron failure, one of the electrodes was ruptured while testing at the 3000 joule level. Since in both cases pressure readings were taken starting at the lowest level of voltages at which an explosive-like discharge could be generated, it was possible to obtain readings of peak pressure as a function of initial energy for both configurations tested.

The overall inductance of the low inductance discharge circuit was evaluated from a current trace obtained by shorting the electrode assembly with a strap. The shorting strap made contact around the complete circumferences of both the anode and the cathode. Calculations based upon the measurements carried out indicated an overall circuit inductance between  $1.5 \times 10^{-7}$  Henries to  $2.8 \times 10^{-7}$  Henries for either of the two electrode assemblies mentioned above. These values are in fair agreement with a value of  $1.4 \times 10^{-7}$  Henries originally estimated<sup>1</sup> for the complete assembly.



Figure 1: Low Inductance Discharge Circuit  
Acoustic Sound Source



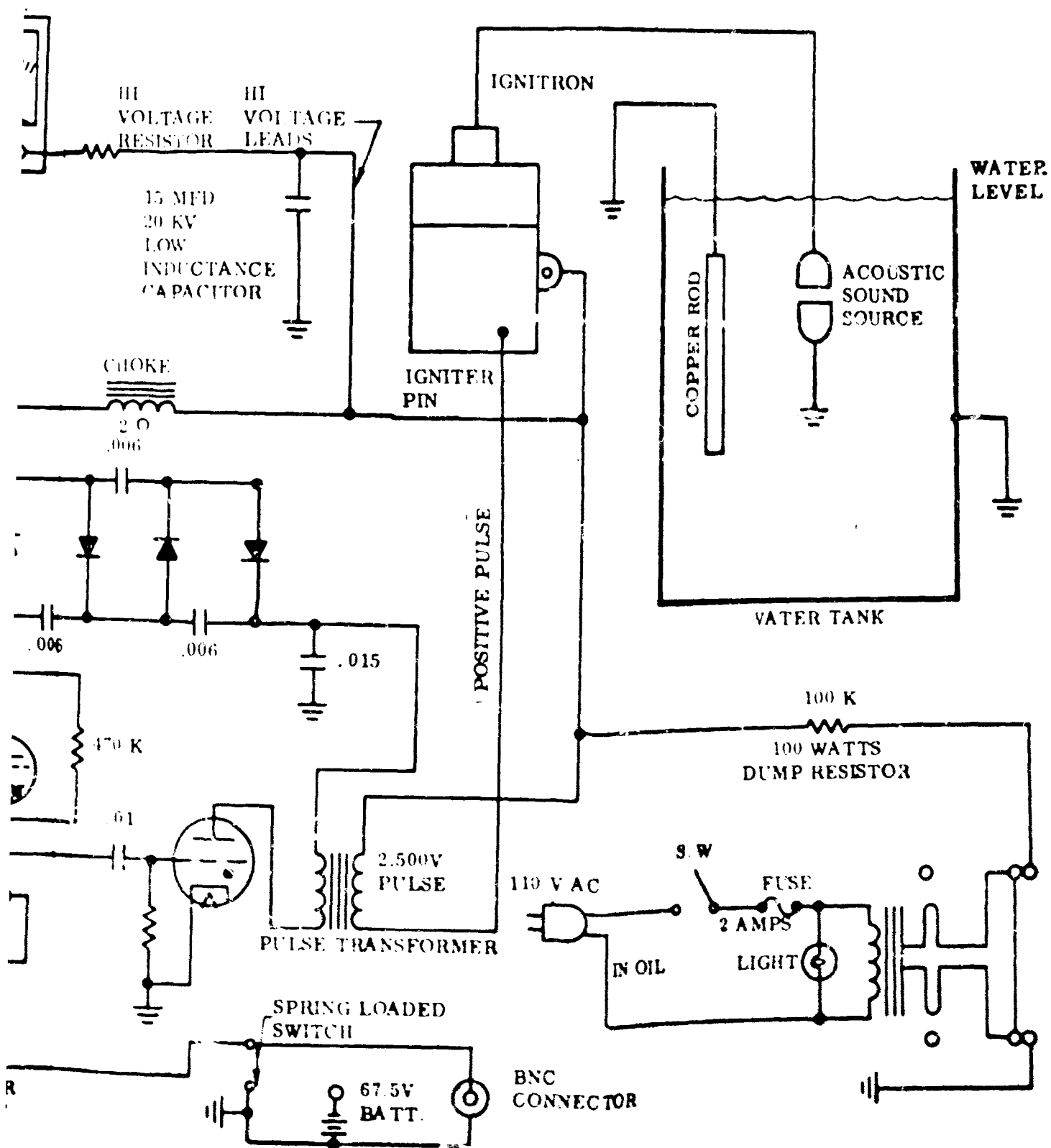


Figure 2: Electric Network Schematic



Figure 3: Capacitor, Ignitron and Electrode Assembly  
With Grounded Housing Removed

Because the cylindrical cathode of the second electrode assembly (shown in Figure 4) was ruptured at the 3000 joule energy level, it was decided to introduce some additional shock isolation. The electrode assembly was therefore modified to incorporate a coil spring in the outer electric current path even though the overall inductance would be increased. Figure 5 shows this modification. The spring and part of the electrode assembly have subsequently (see Figure 15) been potted in an elastic potting compound\*. The potting compound insulates the assembly from the surrounding water and also seals the assembly from water penetration. No pressure data has yet been taken with this latter electrode assembly.

Besides shock isolating the ignitron from the acoustic field generated, it was also necessary to prevent spurious electric discharges from taking place within the coaxial current-carrying assembly surrounding the ignitron. Originally sufficient spacing was provided between current paths to prevent a discharge from occurring between these paths. It was found, however, that when the assembly was immersed in cold water condensation from the entrained air would cause electrical discharges to take place within the enclosure surrounding the ignitron. This spacing was therefore filled with transformer oil. However, it is believed that because of the incompressibility of the transformer oil pressure pulses generated in the surrounding water transferred to the ignitron casing and may possibly have contributed to the failure of one ignitron. The problem of internal arcing was resolved by filling the spacing with a very pliable silicone rubber.\*\* After pouring the silicone rubber into the spacing between conductors, the assembly was degassed under an evacuated environment in a vacuum chamber. Besides electrically isolating the current paths from each other, the silicone rubber also provides some vibration isolation. An additional feature of this technique is that the potting compound provides some hermetic sealing of the ignitron when the evacuated glass envelope of the ignitron breaks. Figure 6 shows the potted ignitron and the shock isolating bellows assembly. No spurious discharges between the ignitron and the surrounding casing have been observed since the ignitron assembly has been potted.

- 
- \* PRC-PR-1431 Type II, Products Research Company, 410 Jersey Avenue, Gloucester City, New Jersey
  - \*\* RTV-S15A Silicone Potting Compound, G. E. Silicone Products Dept., Waterford, Connecticut.

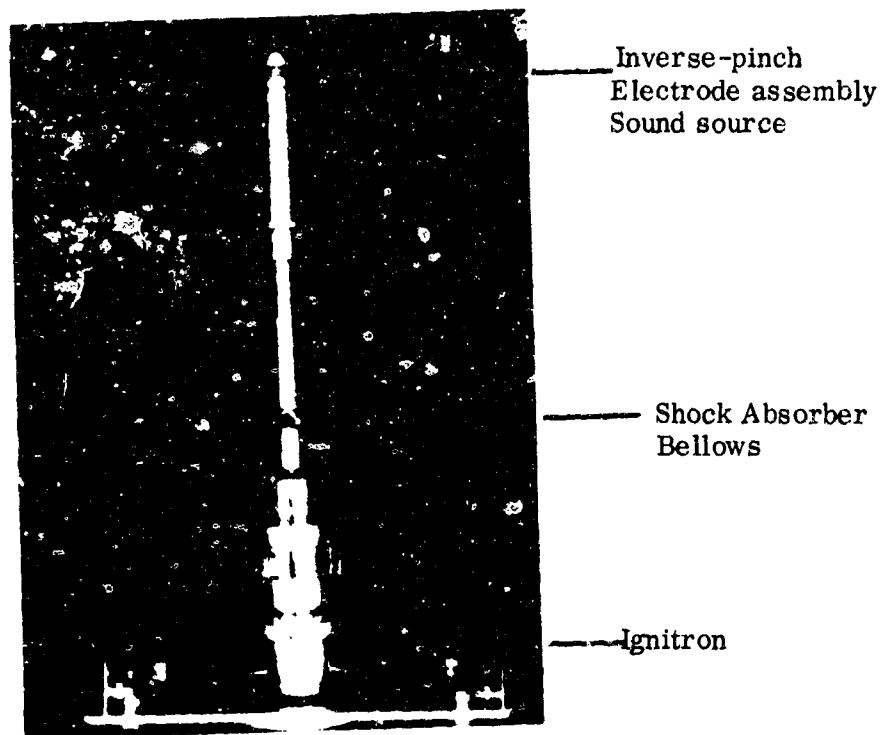


Figure 4: Electrode and Ignitron Assembly With Shock Absorbing Bellows

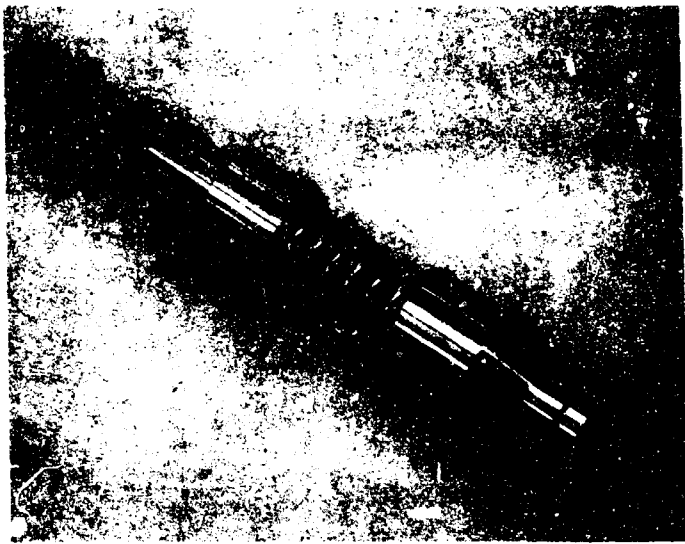


Figure 5: Modified Electrode Assembly With Shock Absorbing Spring

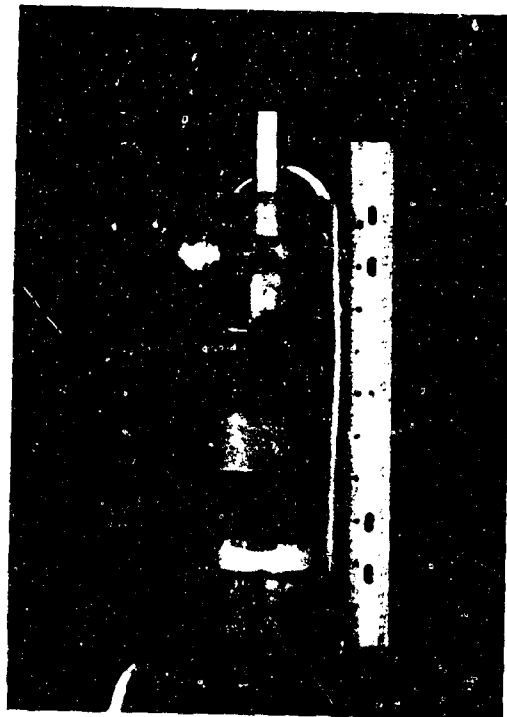


Figure 6: Encapsulated Ignitron and Bellow Assembly

In addition to the above mentioned problems that have been encountered with the low inductance network, a number of insulators in the interelectrode spacing of the inverse-pinch electrodes have ruptured. Teflon, Micarta, Kel-F, and Dynel with a Bakelite ERL-2795 epoxy resin have ruptured within a few discharges. In earlier electrode configurations a satisfactory insulator life has been obtained with Tygon\*. Since Tygon is quite resilient it is difficult to machine into the configuration presently desired. Vacuum cast Adiprene\*\* is therefore being used as the insulator in the present electrode assembly. This latter elastomer can be machined into the configuration desired. After machining, the Adiprene was bonded to the electrodes with THIXON, a product of the Dayton Chemical Products Laboratories, West Alexandria, Ohio. The experimental data reported in this report were taken with the Adiprene insulator located between the electrodes of the acoustic source.

#### B. EXPERIMENTAL RESULTS

The 15  $\mu$  fd capacitor was charged to voltages ranging from 10 KV to 20 KV and subsequently discharged into the inverse-pinch acoustic source. The pressure generated at a distance of three feet from the source was measured with an Atlantic Research Type LC 32 Hydrophone. The data that was obtained with the "rigid" electrode assembly is presented in Table I. Table II presents the data obtained with the electrode assembly which has the shock absorbing bellows incorporated.

---

\* Produced by the U.S. Stoneware Corporation, Akron, Ohio

\*\* Dupont Chemicals Department, E. I. Dupont deNemours & Company, Inc.  
Wilmington, Delaware

**TABLE 1 - EXPERIMENTAL RESULTS**  
**Low Inductance Network (Rigid Electrode Assembly)**

<u>Voltage</u>	<u>Energy, Joules</u>	<u>Peak Pressure at 1 Yd., Psi</u>	<u>Peak Current, Amps</u>	<u><math>20 \log_{10}</math> (Peak Pressure at 1 yd / 1 bar)</u>
10 KV	750	84.5	32,400	135.2
12 KV	1080	169	37,800	141.2
14 KV	1470	169	49,800	141.2
16 KV	1920	206	?	143.1
16 KV	1920	190	?	142.3
16 KV	1920	214	63,500	143.5
18 KV	2430	161.5	70,200	141
18 KV	2430 cd+	206	78,400	143.1
20 KV	3000 cd+	211	83,800	143.1

cd+ indicates that the discharge was not completely critically damped.

**TABLE 2 - EXPERIMENTAL RESULTS**  
**Low Inductance Network**  
**(Shock Absorbing Bellows in Electrical Assembly)**

<u>Discharge</u>	<u>Voltage</u>	<u>Energy, Joules</u>	<u>Peak Pressure at 1 Yd., Psi</u>	<u>Peak Current, Amps</u>	<u><math>20 \log_{10}</math> (Peak Pressure at 1 yd / 1 bar)</u>
2	10 KV	750	85	25,100	135.2
3	10 KV	750	113.8	25,100	137.8
4	12 KV	1080	115.5	29,700 (?)	138
5	12 KV	1080	148	35,000	140
6	14 KV	1470	113.5	47,200	137.8
7	15 KV	1470	137.8	42,000	139.8
8	16 KV	1920	156	48,600	140.7
9	16 KV	1920	214	54,000	143.3
10	18 KV	2430	169.5	59,500	141.2
11	18 KV	2430	174	65,000 cd +	141.8
12	20 KV	3000	201	75,500 cd +	143
13	20 KV	3000	185	75,500 cd +	142.1

The low inductance network data presented in Tables 1 and 2 are compared in Figure 7 with the data that has been obtained with earlier higher inductance discharge networks.

When comparisons are made at a given energy level, it is seen that the low inductance network being reported upon usually generated larger peak pressures one yard from the acoustic source than the pressure that has been generated by any one of the previous discharge circuits that have been used. At voltages of 18 KV and above (i.e., energies greater than 2430 joules) the electric discharge was not critically damped. This factor perhaps explains why the peak pressures that have been recorded above 16 KV are not higher than one might anticipate when compared to the data obtained with the voltage data below 16 KV.

Two typical pressure traces are shown in Figure 8. These traces display the pressure variation three feet from the acoustic source measured in a plane normal to the axis of symmetry of the acoustic source. All of the pressure traces generated by discharges ranging from 10 KV to 20 KV (i.e., a discharge energy ranging from 750 joules to 3000 joules) have essentially the same general form as the two traces shown in Figure 8. The pressure rises rapidly from zero to peak pressure in about 20 microseconds. In another 20 to 30 microseconds the pressure drops from the peak value down to some low value typically 15% to 25% of the peak value. This latter pressure level is reduced by about 50% of its original value over a period of about 400 microseconds after which it drops to very nearly zero. The period during which these pressure variations occur are free from reflections from any of the surfaces of the tank.

The form of the pressure traces that have been observed lend themselves in a rather straightforward manner to spectral analysis. The pressure-time history that has been observed during the work being reported upon can be reasonably well approximated by a series of straight line segments. Appendix A presents in more detail the frequency analysis of these pressure traces which can be approximated by a series of connected straight line segments. The results of the analysis were programmed for a computer to present the acoustic energy per unit area per unit cycle as a function of frequency. It is realized that because of the finite size of the

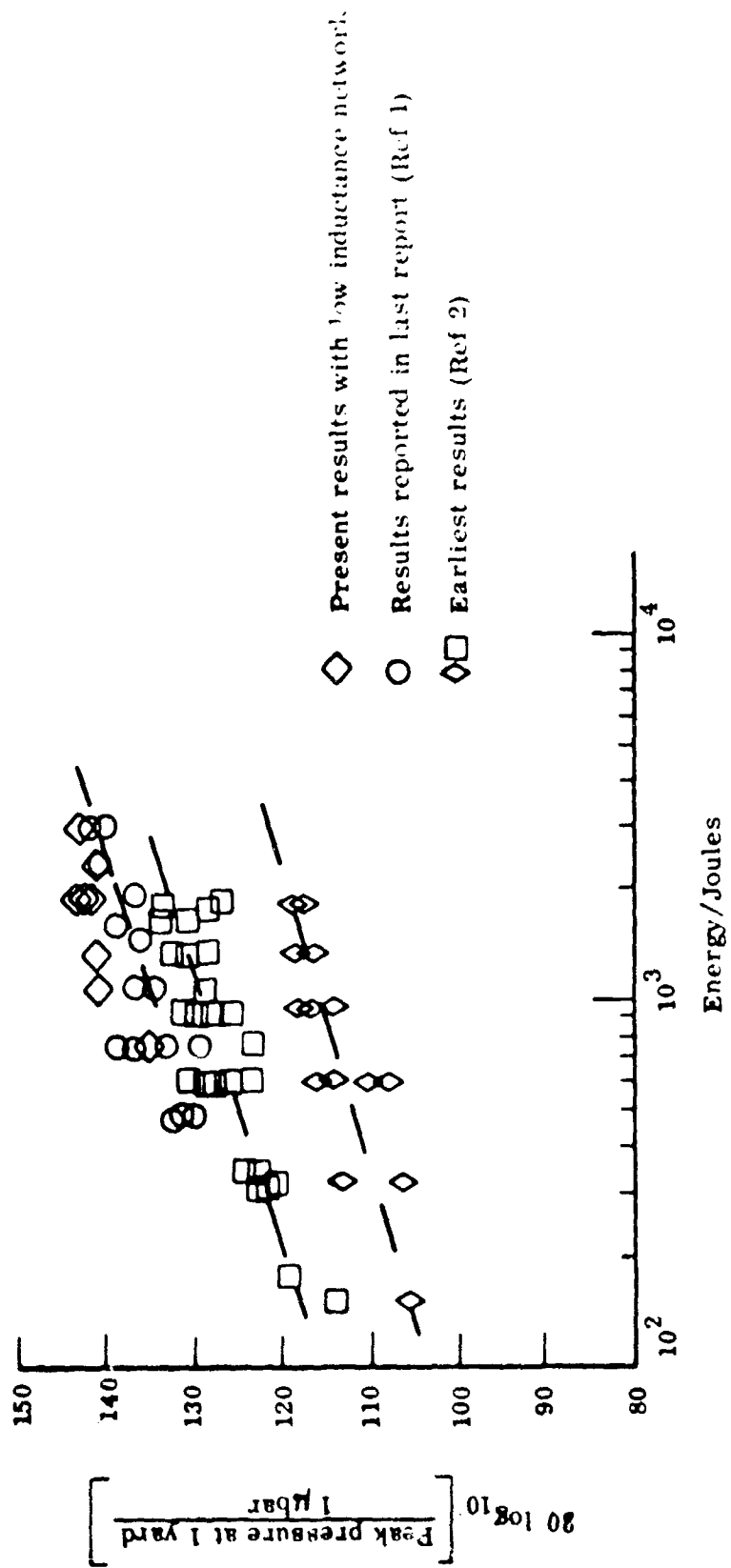
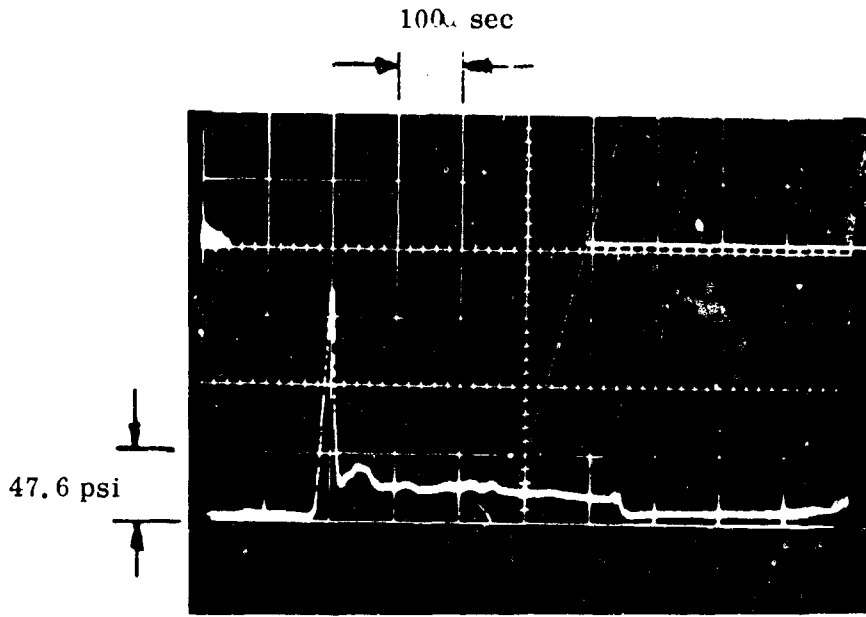
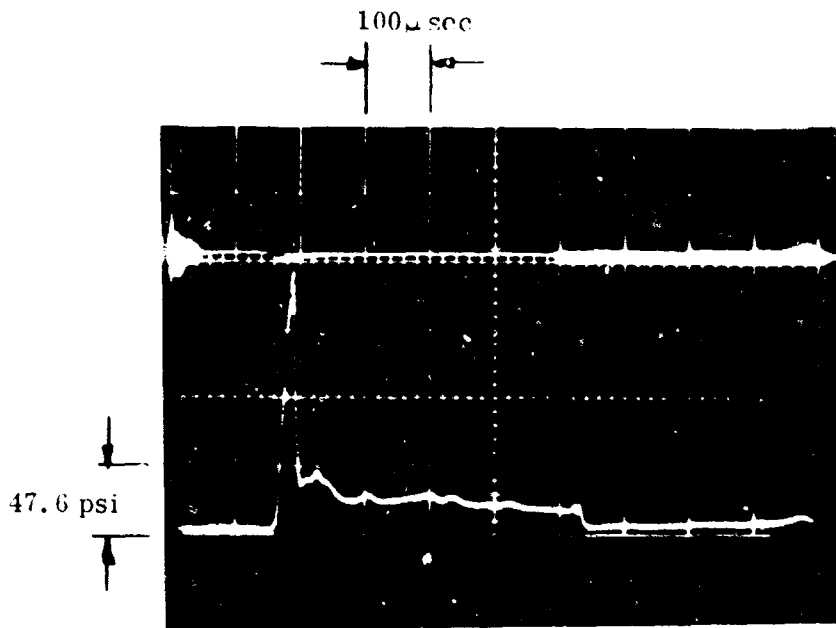


Figure 7 Peak Pressure at One Yard as a Function of Capacitor Energy (Zero Salinity)



12 KV



14 KV

Figure 5: Pressure Traces at 1 yard from the Acoustic Source

tank (8 feet diameter) in which tests were conducted the calculated frequency data below about 2000 Hz is not meaningful. It is hoped that pressure readings in the ocean could be carried out so that the complete spectrum generated by the acoustic source could be had.

Figure 9 presents the results of spectral analyzing the pressure data presented in Figure 8 as well as an additional pressure trace that was taken at 16 KV. Because of the size of the tank in which tests were carried out the calculated energy radiated at low frequencies is not valid. It is not known whether the peak spectral energy density that was generated occurs at about 2800 Hz or if the peak occurs somewhere near 1300 Hz before the energy density variation merges into the correct asymptotic behavior at low frequencies. Tests carried out in either a lake or in the ocean should provide the exact location of the peak of the spectrum as well as the correct asymptotic behavior at low frequencies. Since the variation of pressure with time had essentially the same shape (see Figure 8) in all three cases that have been analyzed, it is not surprising to observe that all three energy spectral variations are similar.

Work is now in progress to determine if the spectral energy distribution can be controllably changed by imposing particular electric current waveforms (i. e. , rate of energy addition) entering the plasma of the acoustic source. The motivation for suspecting the feasibility of varying spectral energy distribution by varying the rate of energy addition is based upon the following considerations. The spectral energy distribution  $S(\omega)$  is determined from an evaluation of the Fourier integral of the temporal pressure variation  $p(t)$  measured some distance from the acoustic source. Hydrodynamically, it is known that this latter temporal pressure variation is a function of the temporal pressure variation at the source. An appropriate equation of state relates the instantaneous pressure in the plasma at the source to the internal energy of the plasma. The instantaneous internal energy, however, is a function of the rate of energy addition and the rate of all forms of energy radiated by the source. Hence by varying the rate of energy addition to the plasma one can expect the temporal pressure variation at the source to be varied and therefore the corresponding pressure variation (i. e. , the spectral energy distribution) some distance from the source. This latter hypothesis is going to be checked with the pulse forming network to be described in the next section.

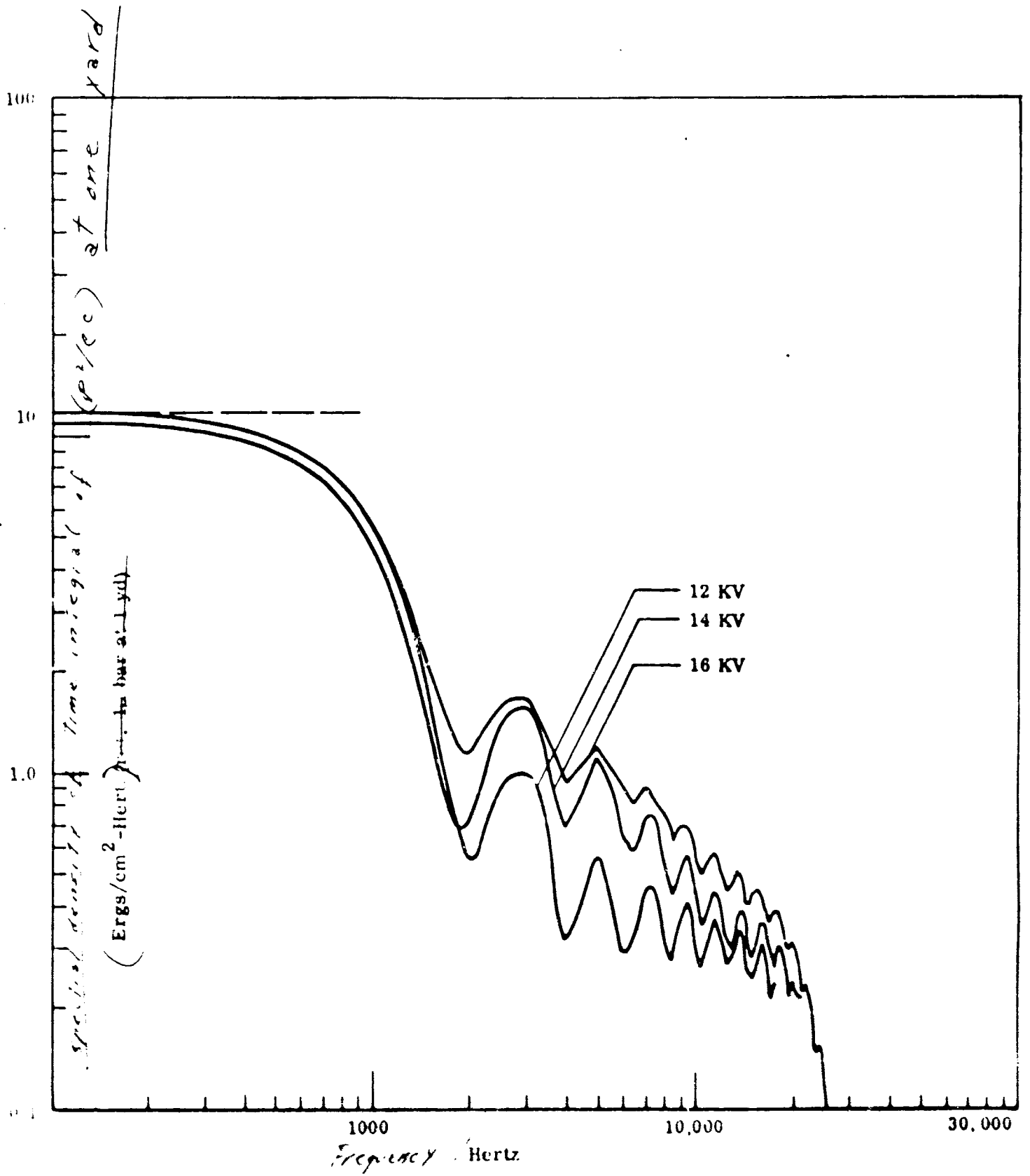


Figure 9. Spectral Analysis of Pressure Traces

## SECTION III - FREQUENCY SPECTRUM SHAPING

### A. INTRODUCTION

The next phase of our work will be devoted, as indicated in the preceding section, to an investigation of the feasibility of controlling the frequency spectrum of the acoustic pulse in the water through variation of the electrical discharge waveform, i.e., the time rate of energy addition to the discharge plasma. The rate of growth of the plasma-water interface directly determines the frequency content of the acoustic signal; the pressure which determines this growth is directly related to the energy input. The relative flexibility in time shaping provided by an electrical energy source compared to explosions or pneumatic systems could prove a most useful advantage of such systems. In particular, the possibility of increasing the low frequency content of the acoustic pulse relative to a simple discharge will be explored.

The method to be used for this study is to consecutively discharge three separate capacitors into the underwater electrode assembly. Provisions have been made for independent control of the time of discharge of each capacitor as well as the charging voltage of each capacitor. These six variables that are available provide sufficient flexibility in generating the waveform of the "forcing" voltage on the electrodes to permit study of the results of use of a wide variety of both single (composite) and closely spaced individual electrical pulses on the acoustic signal. For example, pulses closely spaced relative to the natural frequency of the discharge circuit serve to effectively increase the duration of the pulse (or the period, if the system is underdamped). Differential charging of the capacitors should permit use of rising or falling ramp voltage waveforms to study the effect, for example, of reserving energy until breakdown initiation has been completed. Although complete control is obviously not possible from this pulse forming network, promising results from this system would provide impetus for development of more sophisticated pulse forming techniques.

## B. EXPERIMENTAL ARRANGEMENT

Figure 10 shows a schematic of the layout of the components of the capacitor bank charging and firing circuits. Three Cornell-Dublier low inductance capacitors of 15 $\mu$  fd, 20 KV size, representing thus a total energy capability of 9000 joules, and their associated G. F. GL 7703 ignitron switches, are assembled to a pair of 26-inch diameter low-inductance collecting plates in the configuration shown in Figures 11 and 12. A coaxial cable approximately 20 feet in length leads to the underwater electrode assembly. Preliminary measurements indicate that the inductance of this lead-in cable is approximately  $1 \times 10^{-6}$  Henries.

Return to the use of a fairly long cable, with the concomitant higher inductance has been adopted for operational convenience in development of pulse-shaping techniques. In particular, the mechanical fragility of the ignitrons when directly coupled to the electrodes, as detailed in the preceding section, makes their further use in such arrangements of little value. The results of the pulse shaping investigation, if fruitful, may be readily incorporated into later development of low-inductance configurations when a more reliable electrical switch is obtained. Procurement from the Signalite Corporation (Neptune, New Jersey) of a triggerable sealed spark gap switch which promises to fulfill this requirement has been initiated.

Three pulse generators essentially similar to that shown in Figure 2 have been fabricated for this work, and furnish an approximate 2.5 KV trigger pulse to fire the ignitron switches. A circuit capable of generating two delayed input pulses each controllable from 0-300 microseconds to supply the input to these pulse circuits was designed and constructed. A schematic of this circuit is shown in Figure 13; this unit together with all necessary controls has been assembled into the control panel shown in Figure 14. Considerable attention has been devoted to providing adequate electric shielding and isolation in order to preclude signal coupling and premature triggering of the separate pulse circuits.

The electrode design shown in Figure 5 has been reassembled and attached to a cable and support system as shown in Figure 15. This design which employs the

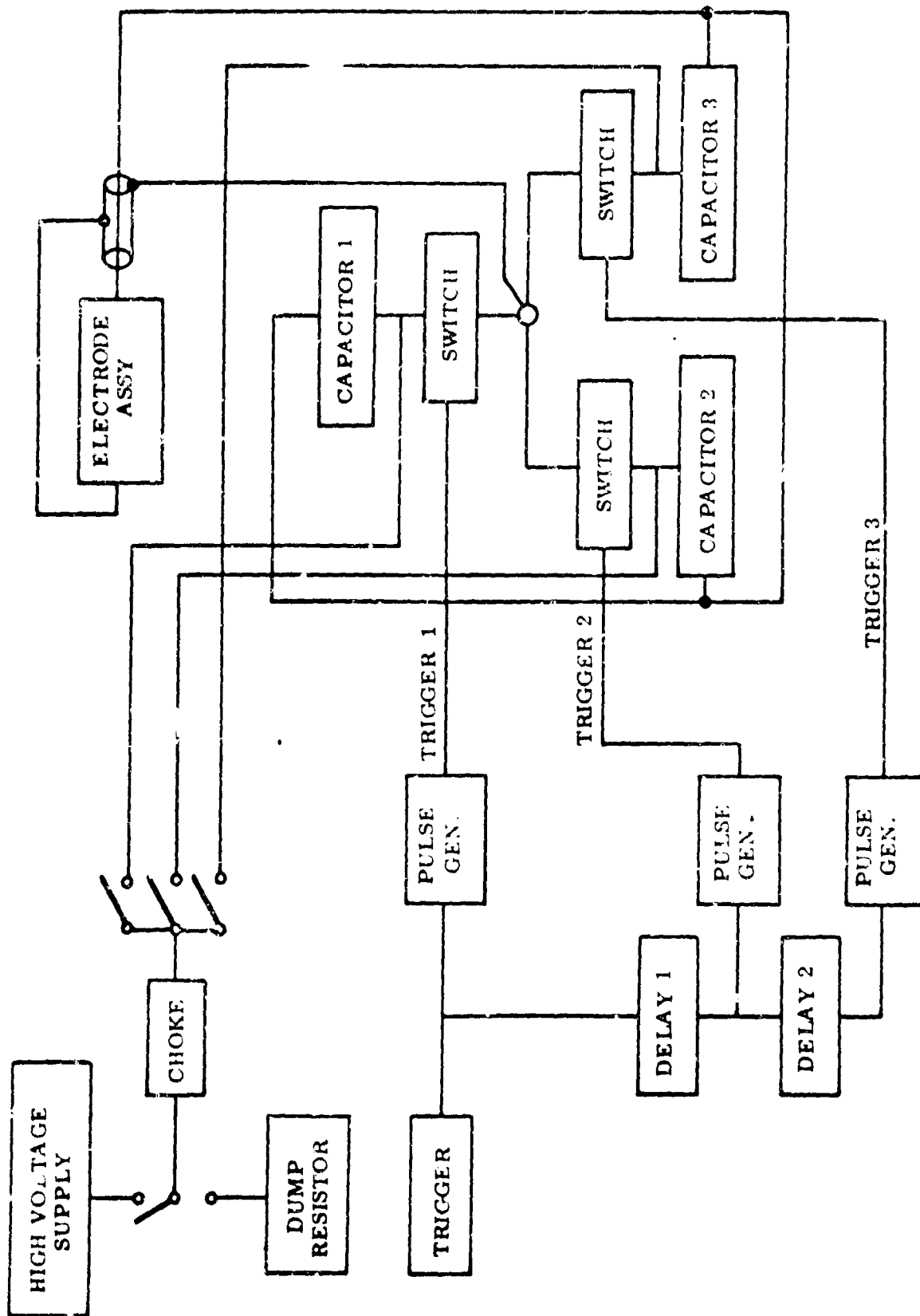


Figure 10. Main Electrical Circuit Schematic

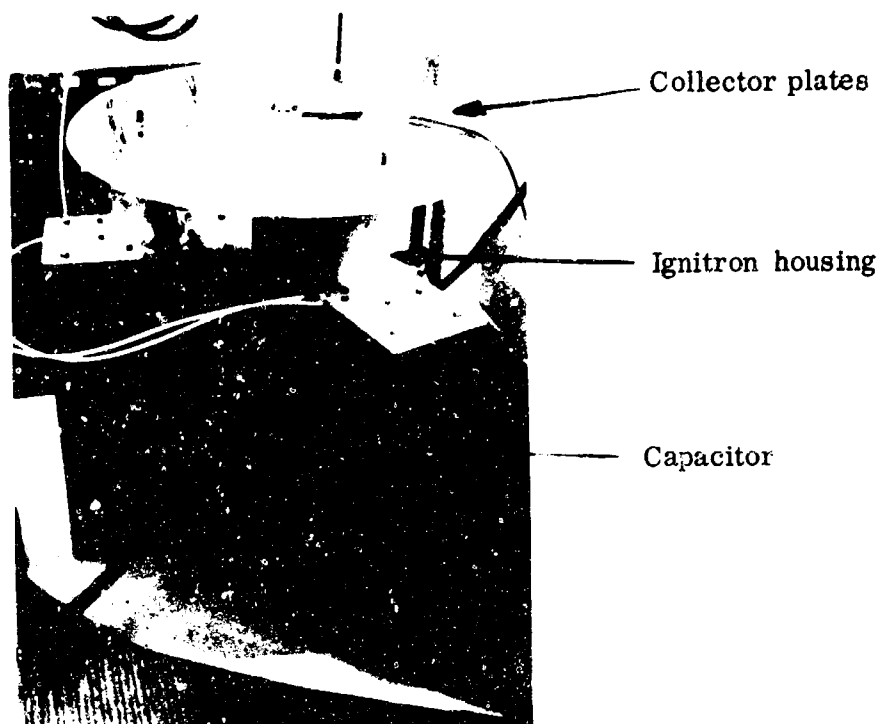


Figure 11: Capacitor Bank Assembly



Figure 12: Ignitron in Housing

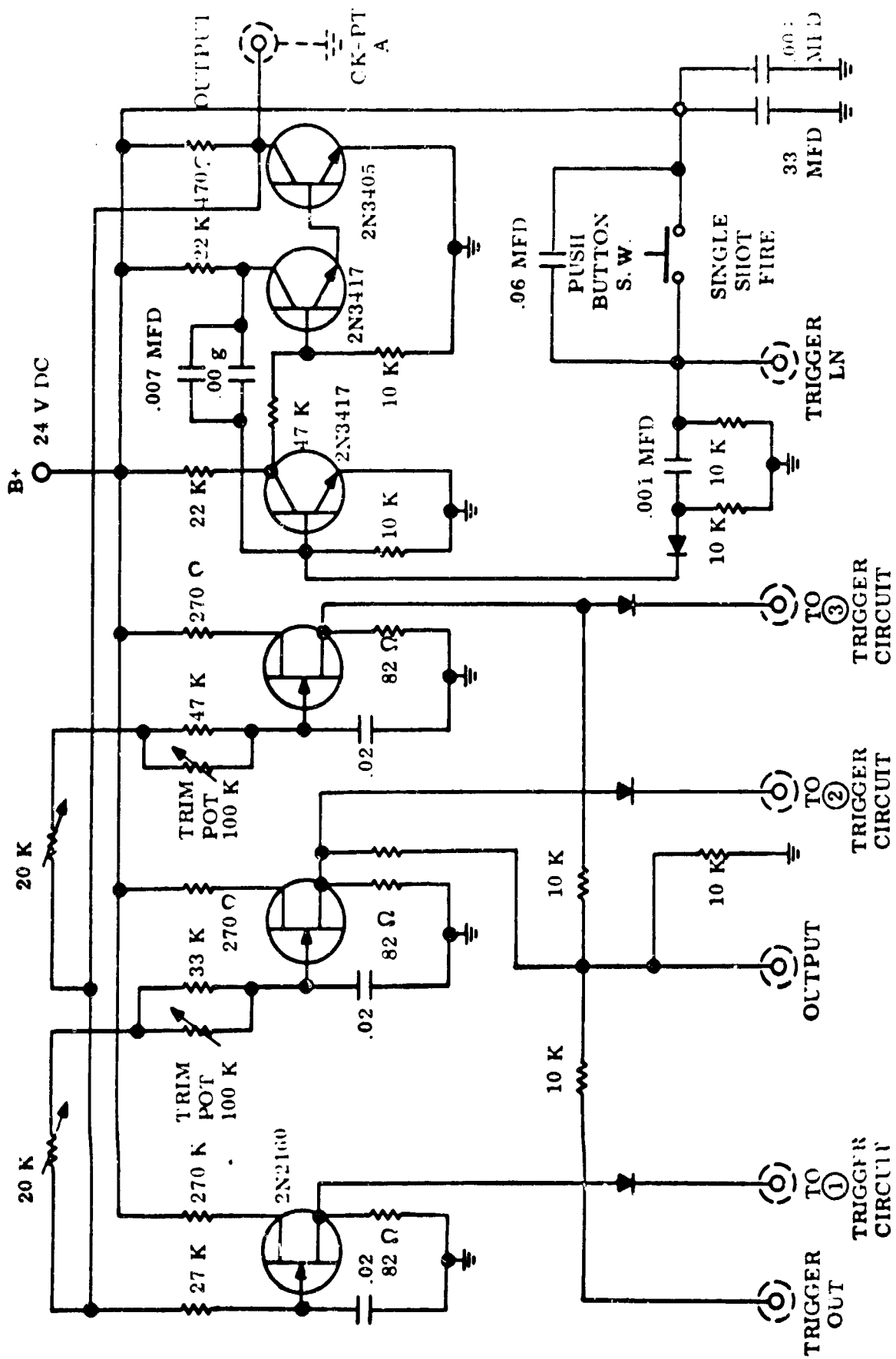


Figure 13. Trigger Delay Circuit

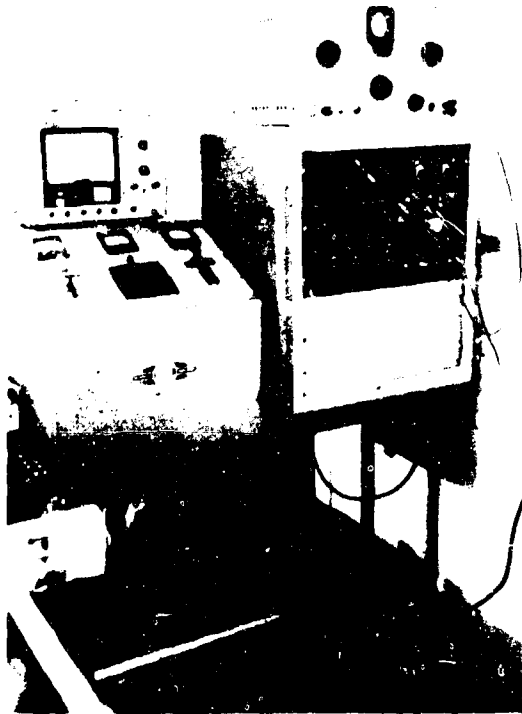


Figure 14: Control Panel

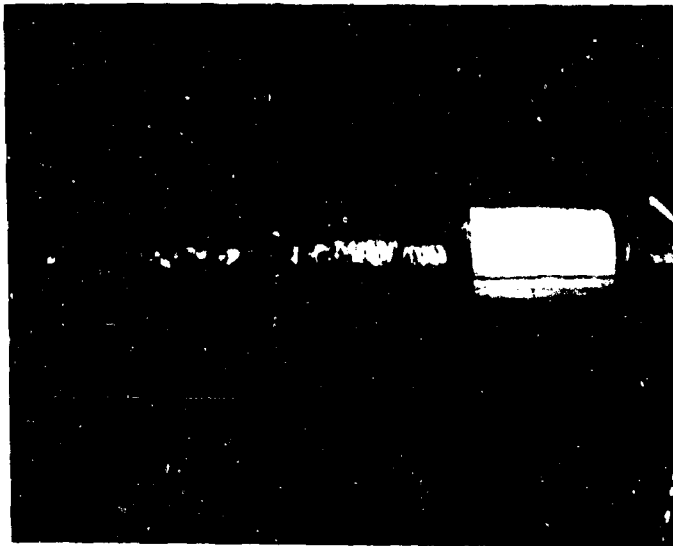


Figure 15: Potted Shock Isolated Electrode Assembly

elastomer Adiprene as an insulation, has performed satisfactorily in the tests carried out. Further evaluation of the integrity of the design will result from the pulse forming studies. The electrode spacing will be the 0.5 inch spacing of the present assembly initially; different insulator spacing will be employed as necessary to control the damping of the discharge after the characteristics of the new electrical circuit have been determined.

The electrical circuit has been completely assembled and is undergoing final checkout. Preliminary results indicate very good control of the sequential firing of each of the three ignitron switches, permitting good control of the pulse shape within the limitations of the technique. Evaluation of the effect of different electrical pulse shapes on the shape and frequency spectrum of the acoustic signal will be initiated in the very near future.

## REFERENCES

1. Guman, W.J., "Study of a Pulsed Underwater Sound Projector," Third Semi-annual Status Report, FHR 2292-3, PCD TR-66-9, 20 June 1966, Fairchild Hiller Corporation, Farmingdale, New York.

## APPENDIX A

### SPECTRAL ANALYSIS OF PRESSURE TRACES RESOLVABLE AS CONNECTED STRAIGHT LINE SEGMENTS

The temporal pressure variations that have been observed (see Figure 8 for example) suggests that an analytic spectral analysis can be carried out by considering the pressure variation to be represented by a series of connected straight line segments. Consider a typical pressure variation to be given in the form shown by Figure A-1.

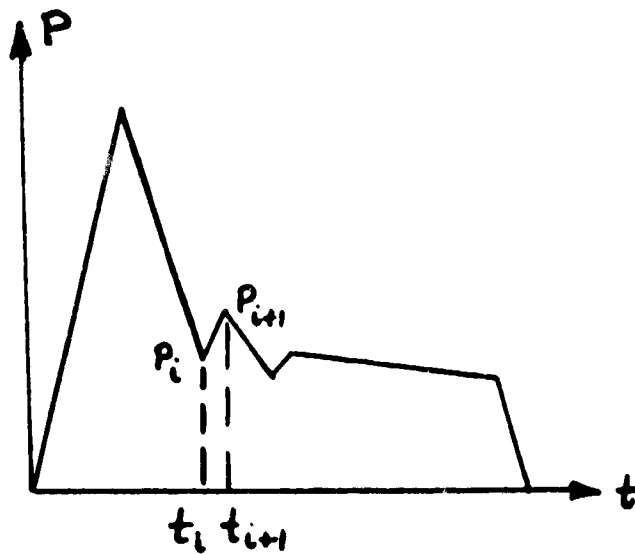


Figure A-1. Typical Pressure Variation

In the interval of time  $\Delta t = t_{i+1} - t_i$  the pressure is given by the relation:

$$p(t) = P_i + \frac{P_{i+1} - P_i}{t_{i+1} - t_i} (t - t_i)$$

This relation is of the form:

$$p(t) = A_i t + B_i$$

with

$$A_i = \frac{P_{i+1} - P_i}{t_{i+1} - t_i}$$

$$B_i = P_i - A_i t_i$$

The energy density flux is defined as:

$$S(w) = \frac{2}{\rho c} \left| F(w) \right|^2$$

with  $\rho$ ,  $c$ , and  $F(w)$  the mass density, sound velocity and

$$F(w) = \int_{-\infty}^{\infty} p(t) e^{-j\omega t} dt = \sum_{i=0}^n F_i(w) = \sum_{i=0}^n \tau_i - j \sum_{i=0}^n B_i$$

respectively. Now

$$\alpha_i = \int_{t_i}^{t_{i+1}} (A_i t + B_i) \cos \omega t dt$$

$$\beta_i = \int_{t_i}^{t_{i+1}} (A_i t + B_i) \sin \omega t dt$$

Integrating these latter two expressions and simplifying the resulting expression gives:

$$\alpha_i = 2 \Delta_i \left\{ (\cos \omega \tau_i) \left( \frac{\sin \omega \Delta_i}{\omega \Delta_i} \right) (P_i + A_i \Delta_i) + (A_i \tau_i) \left( \frac{\sin \omega \tau_i}{\omega \tau_i} \right) (\cos \omega \Delta_i - \frac{\sin \omega \Delta_i}{\omega \Delta_i}) \right\}$$

$$B_i = 2 \Delta_i \left\{ (\sin w \tau_i) \left( \frac{\sin w \tau_i}{w \tau_i} \right) (P_i + A_{i-1}) - (A_{i-1}) \left( \frac{\cos w \tau_i}{w \tau_i} \right) \left( \cos \Delta_i - \frac{\sin w \Delta_i}{w \Delta_i} \right) \right\}$$

with

$$\Delta_i = \frac{t_{i+1} - t_i}{2}$$

$$\tau_i = \frac{t_{i+1} + t_i}{2}$$

$$w = 2 \pi f$$

with  $f$  the frequency.

The spectral energy distribution can then be readily evaluated on a computer by noting that:

$$S(w) = \frac{2}{\rho c} \left[ \left( \sum_{i=0}^n \alpha_i \right)^2 + \left( \sum_{i=0}^n \beta_i \right)^2 \right]$$

These latter relations were used to spectral analyze the pressure distributions presented in Figure 8. The results of this analysis are presented in Figure 9.

The acoustic energy radiated by the acoustic source can be determined from a pressure survey carried out at all points of a spherical surface of radius  $r$  whose center is at the source and subsequently carrying out a double integration over all frequencies and over the surface area surveyed. Only in the very special case of a perfectly spherically symmetric discharge will the energy radiated across a spherical surface of radius  $r$  be given by:

$$E = 4 \pi r^2 \int_0^{\infty} S(w) df$$

An accurate evaluation of the acoustic energy radiated by the source under investigation has yet not been carried out. Such a measurement is most meaningfully carried out in an unconfined environment. Only in such an environment is it possible to have confidence in having determined the correct low frequency portion of the spectrum radiated.